Journal of Petroleum Exploration and Production Technology (2019) 9:525–541
https://doi.org/10.1007/s13202-018-0487-7

ORIGINAL PAPER - PRODUCTION ENGINEERING

A case study of gas-condensate reservoir performance under bottom water drive mechanism

Tung V. Tran[1] · Tu A. Truong[1] · Anh T. Ngo[1] · Son K. Hoang[1] · Vinh X. Trinh[1]

Received: 24 October 2017 / Accepted: 10 May 2018 / Published online: 2 June 2018

Abstract

This case study investigated the effects of formation reservoir properties, aquifer influx, and production scheme on ultimate recovery and production behaviors of a gas-condensate sandstone reservoir Sand20 offshore Vietnam. Optimum production strategy was then formulated to maximize the hydrocarbon recovery while reducing the water treatment cost. The approach focused on the construction of benchmarked radial numerical models to describe the water coning and breakthrough phenomenon and to better understand the impacts of aquifer on deliverability and ultimate recovery of a gas-condensate reservoir. In this study, all factors that have potential impacts on gas and oil ultimate recoveries such as gas production rate, completion length, aquifer size, reservoir horizontal permeability, and permeability anisotropy were investigated. The numerical results showed that for permeability greater than 100 mD, withdrawal rates do not have significant impacts on reservoir gas recovery, while the oil recovery decreases with increasing withdrawal rates. To maximize the ultimate oil recovery, minimize total water production, delay water breakthrough time, and prolong field production life, the wells are recommended to produce at a reasonable low gas flow rate. On the other hand, a minimum gas production rate is required to recover all the reserves to meet the field's production strategy. Aquifer size was found to have no impact on water breakthrough time for this gas-condensate reservoir, but it can have big impact on the recovery factor and the total water production. This study also suggested that perforation interval should be sufficiently long to maximize recovery. Finally, it was found that water–gas ratio does not increase rapidly until approximately 90% of perforation interval is flooded with water.

Keywords Aquifer influx · Water breakthrough · Gas-condensate · Well Performance · Nam Con Son Basin Vietnam

Abbreviations

DR_i	Grid-cell size of ith cell in radial direction (ft)
DZ	Layer thickness (ft)
h	Thickness (ft)
h_{pD}	Completion length (dimensionless)
h_{perf}	Perforation length (ft)
k	Permeability (mD)
k_H	Horizontal permeability (mD)
k_V	Vertical permeability (mD)
M	Aquifer size
N	Total number of cells in radial direction
N_{layer}	Total number of layers in axial direction
P	Pressure (psia)
P_e	Pressure at the outer boundary (psia)
P_{ini}	Initial reservoir pressure (psia)
PV_g	Pore volume of gas (STB)
P_{wf}	Bottom-hole flowing pressure (psia)
q	Production rate (MMscf/day)
q_g	Gas production rate (MMscf/day)
r	Distance from wellbore in radial direction (ft)
r_e	Reservoir external radius (ft)
r_w	Wellbore radius (ft)
s	Skin factor
S_{wir}	Irreducible water saturation
V_{aq}	Volume of aquifer (STB)
μ	Viscosity (cP)

✉ Tung V. Tran
tungtv@biendongpoc.vn

[1] Bien Dong Petroleum Operating Company, 3rd Floor PetroVietnam Tower, 1-5 Le Duan Street, Ben Nghe Ward, Ho Chi Minh City, Vietnam

Introduction

In a gas-condensate reservoir, the liquid dropping out from the gas occurs when well bottom-hole pressure (BHP) falls below dewpoint pressure. The dropped-out liquid near the wellbore not only is a loss of valuable liquid of heavier

components, but also creates a blockage lowering well deliverability. Reduction in well deliverability due to retrograde condensation has been critically studied over decades (Hinchman and Barree 1985; Banum et al. 1995; El-Banbi et al. 2000). Fevang and Whitson (1996) showed that the loss in well deliverability of gas-condensate wells can be calculated accurately using a pseudopressure method. If the traditional method is used to calculate rate (mobilities evaluated at gridblock pressure), the loss in well deliverability will be under-predicted. Singh and Whitson (2010) also verified the validity and accuracy of the pseudopressure method for layered systems with significant heterogeneity in permeability and gas-condensate composition. Tran et al. (2015) used both pseudopressure and local grid refinement to model condensate-banking phenomenon, and then applied to horizontal and hydraulic fracturing design.

When gas-condensate reservoirs are under a bottom natural aquifer or water influx, the condensate banking will be reduced thanks to pressure maintenance. The effects of water influx in gas and retrograde condensate reservoirs have been studied in the past (Agarwal et al. 1965; Ali 2014; Hower et al. 1992; Izuma and Nwosu 2014; Ogolo et al. 2014). Depending on the size and strength of the aquifer, the ultimate gas and oil recoveries can significantly increase in a gas-condensate reservoir (Ali 2014). However, uncontrolled water production can kill gas wells, leaving a significant amount of gas in the reservoir. Reservoir parameters such as vertical permeability, aquifer size, non-Darcy flow effect, density of perforation, and flow behind casing have important effects on water coning and water production in gas reservoirs with bottom water drive (Armenta 2003). To model the condensate banking or water influx effects on gas-condensate reservoirs, both Cartesian and radial models have been used in the previous studies. However, to the authors' knowledge, the workflow to build a benchmarked simulation model for gas-condensate reservoir is not available. In this paper, we proposed a workflow to build a benchmarked model for a gas-condensate reservoir under bottom water influx. Then, an extensive study on effects of water aquifer and reservoir factors on ultimate recoveries of gas-condensate reservoirs was performed.

Methodology

To describe accurately the effects of bottom water influx on gas-condensate reservoir production, it is crucial to build a benchmarked simulation model. Sand20, the target reservoir of this study, is a relatively homogeneous and isotropic sandstone reservoir with thickness of approximately 100 ft and horizontal permeability on the order of 800 mD. Therefore, a radial model is reasonable to study this reservoir.

In this study, a fine-grid radial simulation model was constructed and calibrated. Once the benchmarked radial simulation model was achieved, sensitivity studies were performed to investigate the effects of depletion scheme and reservoir property parameters on the ultimate recoveries. The investigated factors were gas withdrawal rate, completion length, aquifer size, reservoir horizontal permeability, and permeability anisotropy. From the results of the sensitivity studies, an optimum production scheme was recommended to maximize ultimate recoveries while reducing total water production.

Model calibration

In this study, a benchmarked fine-grid radial model for gas-condensate reservoirs under bottom water influx was obtained by calibrating with available analytical radial solutions. Next, the model was tested for convergence in both radial and axial directions. Specifically, the workflow consists of:

1. calibration with analytical solution for a single-layer radial model with a slightly compressible fluid under steady-state flow and a constant pressure outer boundary;
2. grid convergence test for the single-layer radial simulation model with the actual gas-condensate fluid;
3. grid convergence test for gas-condensate radial simulation model with bottom water influx.

To the best of the authors' knowledge, analytical radial solutions for highly compressible fluids, e.g., gas or gas-condensate, are not available. In fact, the only available analytical radial solution relevant to this reservoir simulation study is the classical steady-state flow of a slightly compressible fluid with a constant outer boundary pressure. Therefore, the radial model was first calibrated against this analytical solution to an accuracy level of 1% for pressure distribution around the wellbore. The calibrated grid was then tested for convergence in both the radial direction and the axial direction. Specifically, the calibrated radial model was found to converge in radial flow using gas-condensate fluid. Moreover, the calibrated grid was also found to be similar to that used previously by Singh and Whitson (2010) in a study on gas-condensate reservoirs. After successfully passing the convergence test in the radial direction, the calibrated grid was tested for convergence in the axial direction. Since the actual reservoir was under bottom water drive, an aquifer was added to the bottom of the radial model. Different layer thicknesses were used to determine convergence and numerical stability thresholds. Based on the results, a layer thickness was selected to satisfy both convergence and

numerical stability requirements. After the calibration and convergence tests, the fine-grid radial simulation model was considered as benchmarked and was used for actual reservoir analyses. In the future, when other analytical radial solutions become available, the calibration process will be updated accordingly.

Calibration with analytical solution for a single-layer radial model with a slightly compressible steady-state flow and a constant pressure outer boundary

For a reservoir with slightly compressible steady-state flow, the radial flow equation is

$$P - P_{\mathrm{wf}} = \frac{q\mu}{2\pi kh}\left(\ln\frac{r}{r_{\mathrm{w}}} + s\right), \tag{1}$$

where P is the pressure at radial distance r, P_{wf} is the bottom-hole flowing pressure, q is the production rate, μ is fluid viscosity, k is reservoir permeability, h is reservoir thickness, r_{w} is wellbore radius, and s is skin factor. With a constant pressure outer boundary P_{e}, we have

$$P_{\mathrm{e}} - P_{\mathrm{wf}} = \frac{q\mu}{2\pi kh}\left(\ln\frac{r}{r_{\mathrm{w}}} + s\right). \tag{2}$$

From Eqs. 1 and 2, the pressure, P, at any distance, r, can be calculated by

$$P = \left(P_{\mathrm{e}} - P_{\mathrm{wf}}\right)\frac{\left(\ln\frac{r}{r_{\mathrm{w}}} + s\right)}{\left(\ln\frac{r_{\mathrm{e}}}{r_{\mathrm{w}}} + s\right)} + P_{\mathrm{wf}}. \tag{3}$$

To calibrate with the analytical solution above, a numerical finite-difference radial model was constructed using the commercial Eclipse 300 compositional simulator. The fine-grid radial simulation model had one layer with a thickness of 100 ft, reservoir external radius of 6500 ft, and one producer in the center of the reservoir. Water was used as the saturating fluid. To model a reservoir with a constant pressure outer boundary, an enormous aquifer was added at the outermost boundary of reservoir. Other reservoir parameters are summarized in Table 1. The number of grid cells in the radial direction was optimized, so that the numerical simulation pressure had less than or equal to 1% error compared to the analytical results. The general view of the radial model is shown in Fig. 1.

Table 1 Reservoir parameters for simulation model

Parameter	Value
Porosity	0.25
k_{H} (mD)	800
P_{ini} (psia)	10,500
r_{w} (ft)	0.354
Skin	0

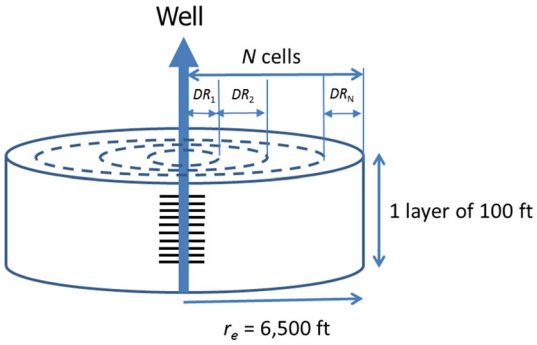

Fig. 1 General view of the radial simulation model

The cells need to be highly refined near wellbore to achieve the accuracy target. The first model contained 150 cells in radial direction, in which the 100 innermost cells had the same small grid-cell size of 0.003 ft and the last 50 cells had exponentially distributed sizes. As shown in Fig. 2, the max error was only 0.6%, which was less than the error target of 1%. Therefore, the simulation model was coarsened while still maintaining the accuracy target. The number of grid cells reduced from 150 to 51, in which only the innermost cell had the size of 0.003 ft and the next 50 cells had exponentially distributed grid-cell sizes. The error was practically the same as in the previous case, as shown in Fig. 2. Next, the grid-cell size of the innermost cell, DR_1, was gradually increased while maintaining the error target of 1%, as shown in Fig. 3. At the value of 0.3 ft, the max error was almost equal to 1%, which still satisfied the error target. However, when $\mathrm{DR}_1 > 0.3$ ft, the error at near wellbore exceeded the error target of 1%. To ensure model robustness, a value of 0.177 ft ($=0.5\ r_{\mathrm{w}}$) was used for the grid-cell size of the innermost cell.

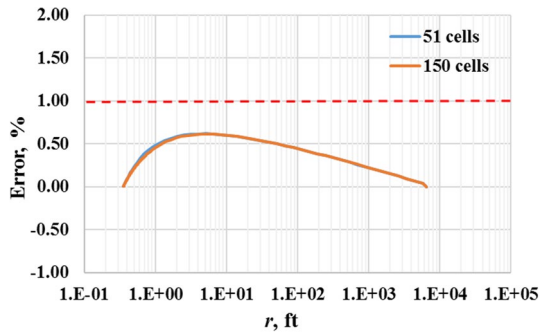

Fig. 2 Error vs. distance from wellbore for two cases: 150 cells and 51 cells

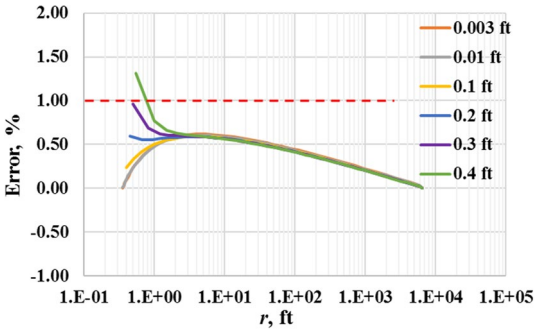

Fig. 3 Error vs. distance from wellbore for different sizes of the innermost cell

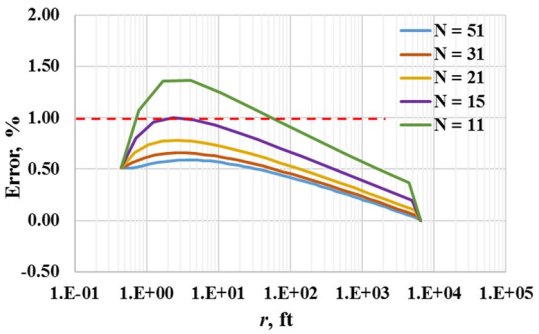

Fig. 4 Error vs. distance from wellbore for different total number of cells

With $DR_1 = 0.177$ ft, the total number of cells with exponentially distributed size in radial direction was varied to investigate its influence on the pressure error. As shown in Fig. 4, when the total number of cells, N, was greater than or equal to 15, the error target of 1% was achieved. Therefore, the minimum total number of cells in radial direction of 15 was required to achieve the error target of 1%.

The effects of other parameters such as layer thickness, reservoir permeability, and porosity on the error were also investigated. The results showed that the error is independent of layer thickness, reservoir permeability, and porosity, as displayed in Fig. 5a through c, as expected from Eq. 3.

Moreover, when the reservoir radius increases, the required minimum total number of cells in radial direction also increases, as summarized in Table 2 and Fig. 6.

Grid convergence test for the single-layer radial simulation model with the actual gas-condensate fluid

Next, the fine-grid radial simulation model containing 15 grid cells in radial direction with reservoir radius of 6500 ft, single layer with a thickness of 100 ft, and the grid-cell size of the innermost cell of 0.177 ft, was used for grid-cell converge test with the actual gas-condensate fluid of the studied reservoir Sand20. Three cases were run with a total of 15, 20, and 30 cells. As shown in Fig. 7, both gas and oil productions from three cases were the same. Therefore, convergence was achieved with 15 cells. Consequently, the radial model with 15 cells and grid-cell size of the innermost cell of 0.177 ft (≈0.054 m) is suitable to simulate Sand20 gas-condensate reservoir. For comparison, this model is comparable with that in Singh and Whitson (2010), as summarized in Table 3.

Grid convergence test for gas-condensate radial simulation model with bottom water influx

In this convergence test, an aquifer was added at the bottom of the fine-grid radial simulation model containing 15 grid cells with reservoir radius of 6500 ft, total thickness of 100 ft and the grid-cell size of the innermost cell of 0.177 ft. The well was perforated only top half of the reservoir (=50 ft). The 100 ft thickness of the reservoir was divided into layers with the same thickness. The number of layers in axial direction, N_{layer}, varied from 2 to 200 or the thickness of each layer, DZ, varied from 50 to 0.5 ft. Sand20 gas-condensate reservoir was run with input data, as summarized in Table 4.

Figures 8, 9, 10, and 11 show the pressures and fluid production of models with different numbers of layers for Sand20. As shown in Figs. 8, 9, 10, and 11, the convergence was reached when $N_{layer} \geq 10$. On the other hand, when $N_{layer} \geq 30$, instability was observed on water production rate. Figures 12, 13, 14, and 15 display the water saturation at near wellbore along vertical depth and water saturation along a reservoir radius at different production times. The water saturation results indicated that the convergence was reached when $N_{layer} \geq 20$. However, instability was observed on water saturation profile at near wellbore when $N_{layer} \geq 70$. Overall, the convergence was reached when the number of layers was at least 20. Nonetheless, when the number of layer was greater than or equal to 30, model instability started to occur. Detailed studies for number of layers from 20 to 28 were then conducted, as summarized in Fig. 16. It was found that instability occurred for number of layers greater than 20. Therefore, for Sand20, it is recommended that the number of layers of 20 is used (thickness of each layer is 5 ft).

In summary, after analytical calibration and convergence tests, a benchmarked model was achieved for Sand20 gas–condensate reservoir with bottom water influx. This benchmarked model is the fine-grid radial simulation model, which contains:

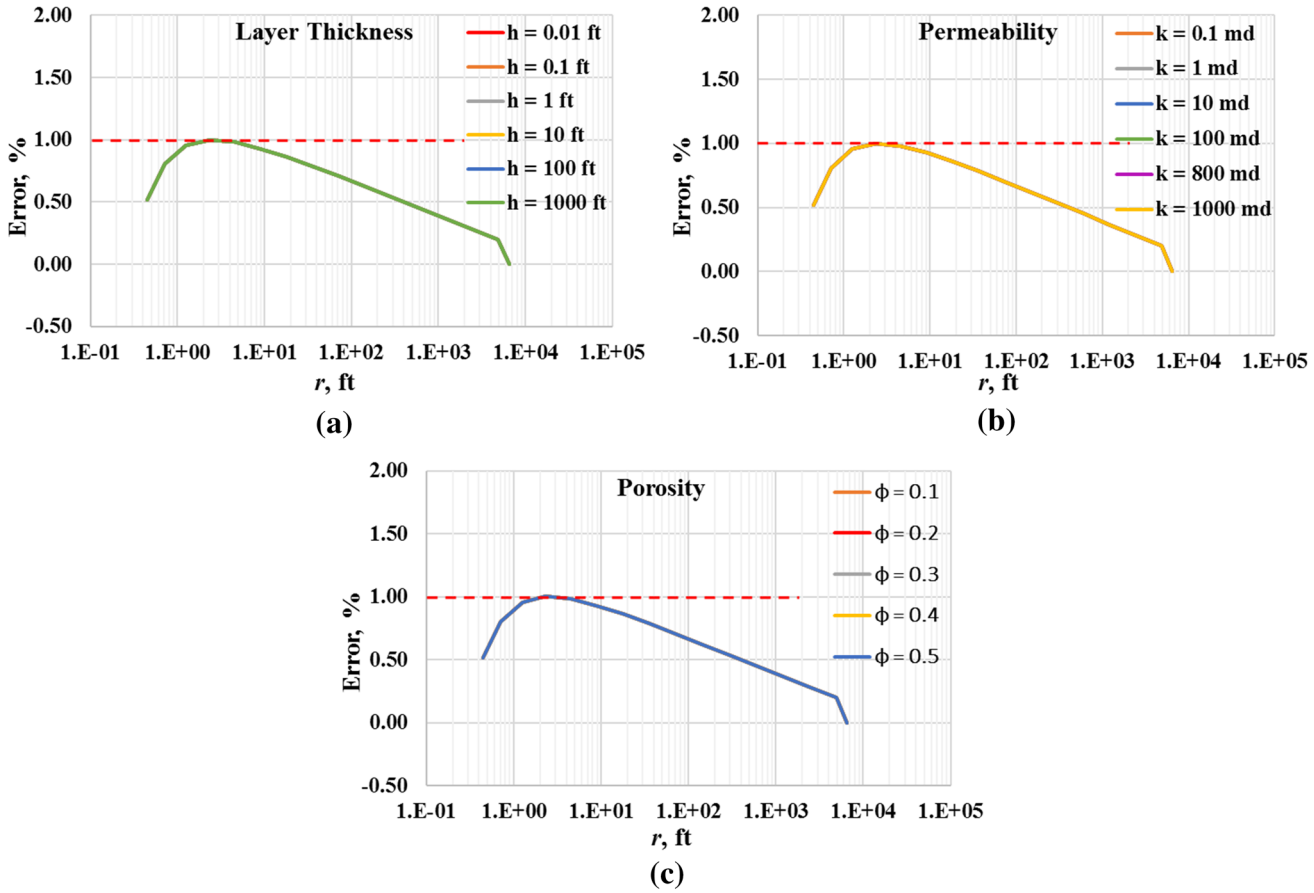

Fig. 5 Error vs. distance from wellbore for different layer thicknesses, permeabilites, and porosities

Table 2 Results of minimum total number of cells with different reservoir external radius for the target error of 1%

$\ln(r_e/r_w)$	r_e (ft)	Number of cells
5.6	100	12
7.3	500	13
8.6	2000	14
9.8	6500	15
10.9	20,000	16

1. 15 exponentially distributed grid-size cells in the radial direction.
2. The grid-cell size of the innermost cell is 0.177 ft ($=0.5r_w$).
3. The thickness of each layer in axial direction is 5 ft.

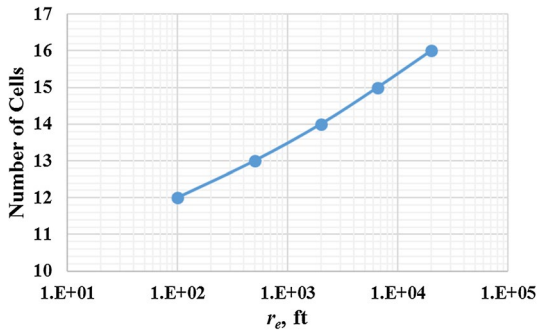

Fig. 6 Minimum total number of cells vs. reservoir external radius for the target error of 1%

Applications to Sand20 gas-condensate reservoir

Sand20 is a gas-condensate sandstone reservoir located in Nam Con Son basin, offshore Vietnam. The reservoir forms a large submarine fan with very high net-to-gross

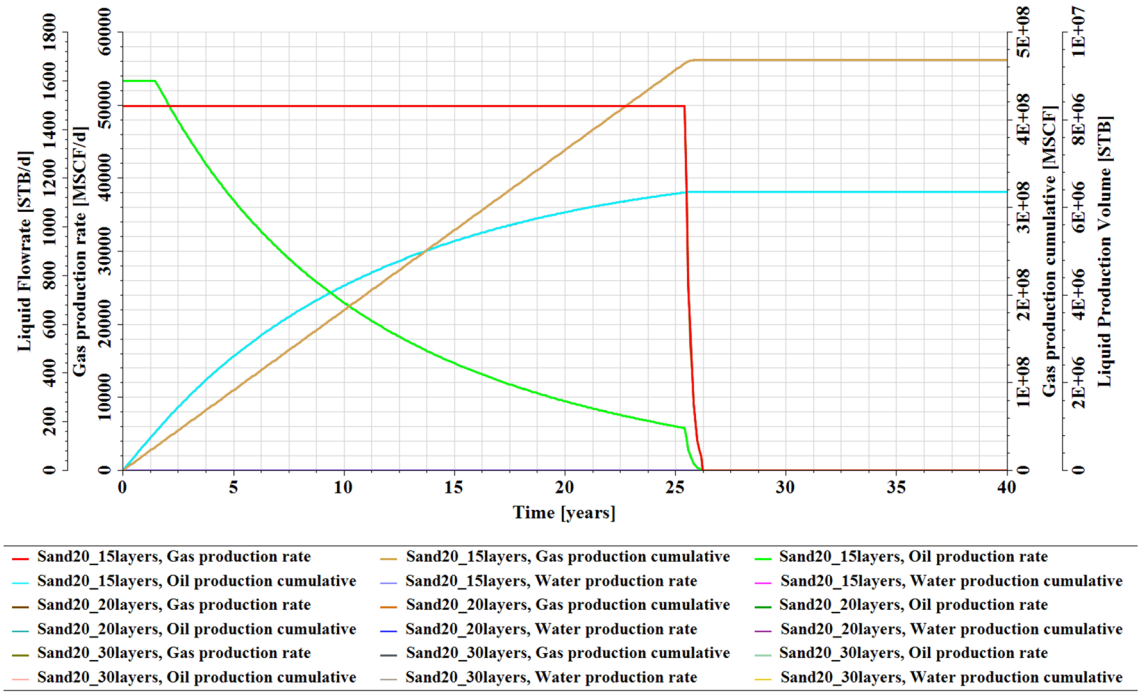

Fig. 7 Gas and oil productions for Sand20 gas condensate for three different total cells: 15, 20, and 30

Table 3 Model parameters comparison between in this study and in Singh and Whitson (2010)

Simulation model	In this study	Singh and Whitson (2010)
Model type	Radial	Radial
Reservoir type	Gas condensate	Gas condensate
CGR (STB/MMscf)	32	60, 90, 175, 250
Size of the innermost cell (m)	0.054	0.05
Number of grid cells in radial direction	15	20
Thickness (m)	30.48	32
Reservoir external radius (m)	1980	900

Table 4 Simulation input data for Sand20 gas-condensate reservoir

Parameter	Value
Reservoir	Sand20
Porosity	0.25
S_{wir}	0.19
k_H (mD)	800
P_{ini} (psia)	7200
r_w (in)	4.25
Skin	0
V_{aq} (STB)	4.50×10^9
Max q_g (MMscf/day)	50
Initial CGR (STB/MMscf)	32

ratio from 0.89 to 1.0, high porosity from 23 to 27%, low water saturation in pay zone, and good permeability from 100 to 800 mD. Conventional cores were available from one of the development wells and both routine and special core analyses were conducted on preserved core samples. Fluid samples were also collected at test separator conditions for PVT laboratory characterization.

Sensitivity studies were carried out to investigate the effects of production and reservoir factors on the ultimate recoveries in Sand20 gas-condensate reservoir with bottom water influx. The base radial simulation model for sensitivity study consisted of 15 exponential distributed size cells in the radial direction with a reservoir external radius of 2580 ft (to honor volumetric estimate of HCIIP per well) and 20 layers in axial direction with the same layer thickness of 5 ft. The grid-cell size of the innermost cell was 0.177 ft ($=0.5r_w$). From routine core analysis,

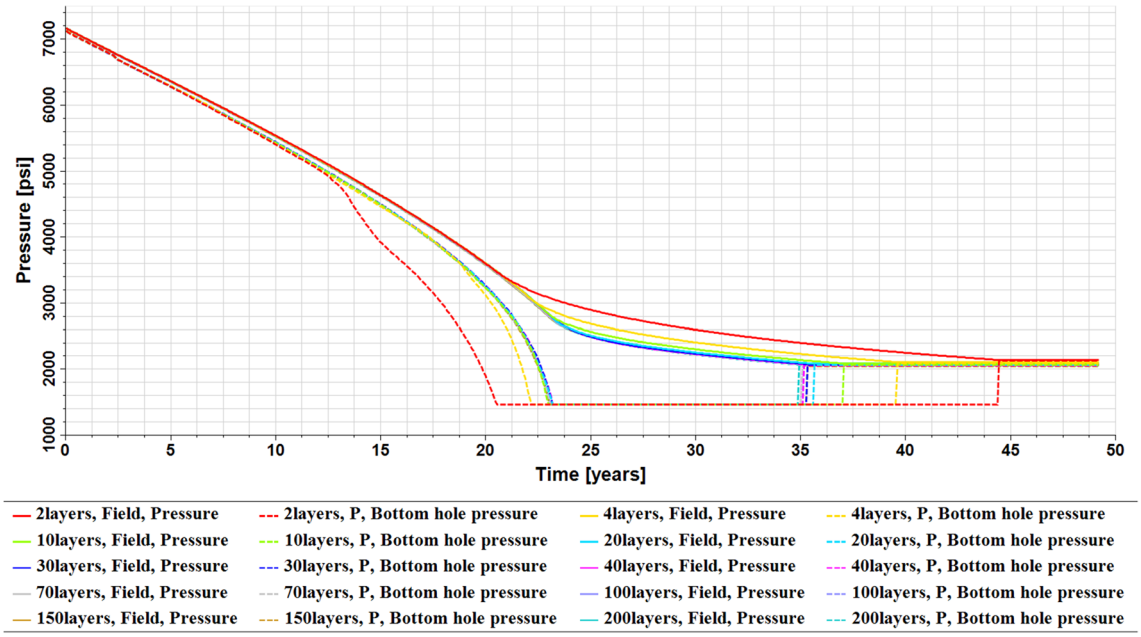

Fig. 8 Reservoir pressure and bottom-hole flowing pressure for models with different layers

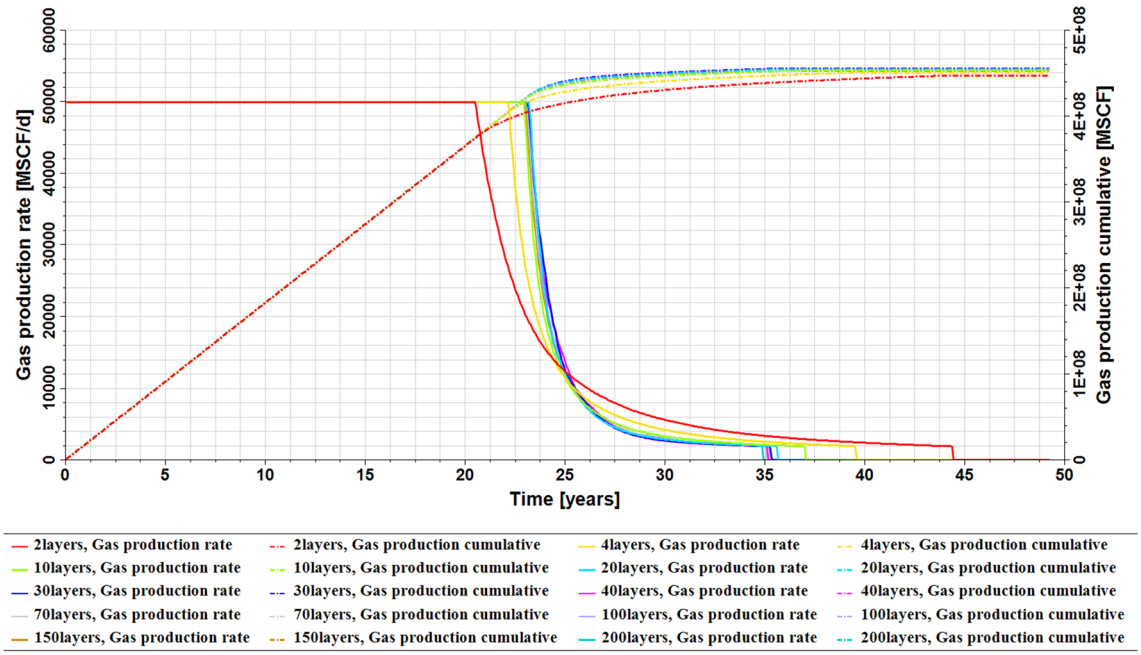

Fig. 9 Gas production rate and cumulative gas production for models with different layers

representative reservoir horizontal permeability and porosity were 800 mD and 0.25, respectively. The vertical-to-horizontal permeability ratio was 0.9 also from experimental results. At the bottom of the radial model, an aquifer of 1.125 billion barrels of water was added. The size of the aquifer for the base radial model was obtained from history matching results of Sand20. Aquifer size, *M*, is defined as the ratio of the volume of the aquifer to the gas pore volume. In the base case, the aquifer size was approximately 15. The Sand20 gas-condensate fluid model with the initial CGR of 32 STB/MMscf (GOR of 31,250 scf/STB) was also used for this study. The simulation model had one producer in the center of the reservoir. The well was perforated over a continuous interval of 50

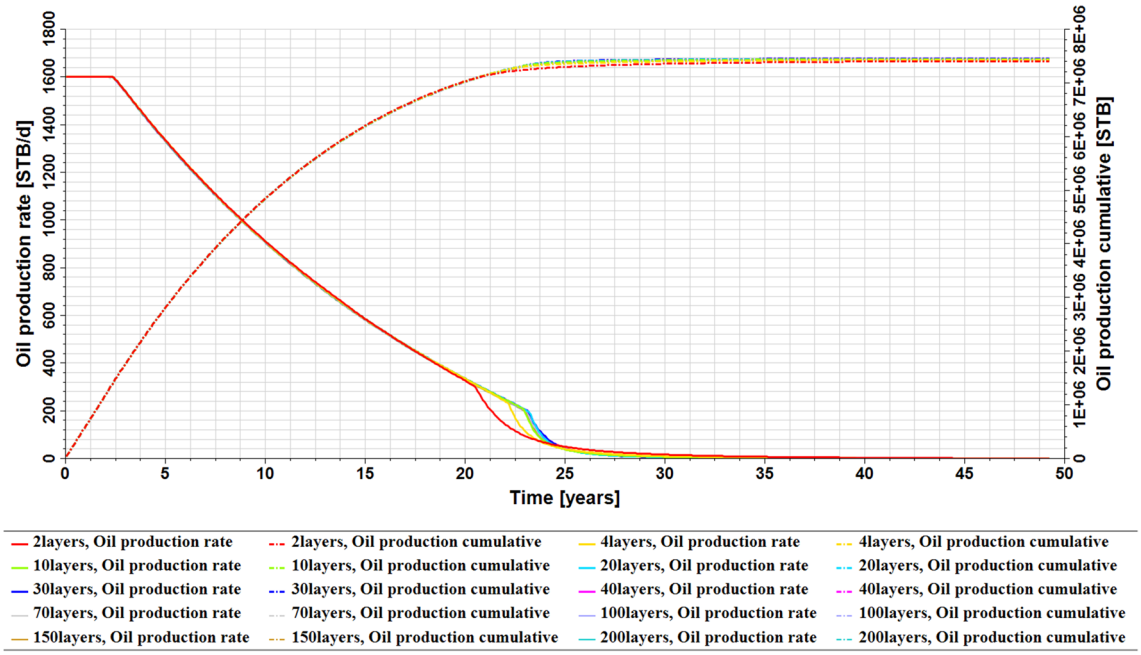

Fig. 10 Oil production rate and cumulative oil production for models with different layers

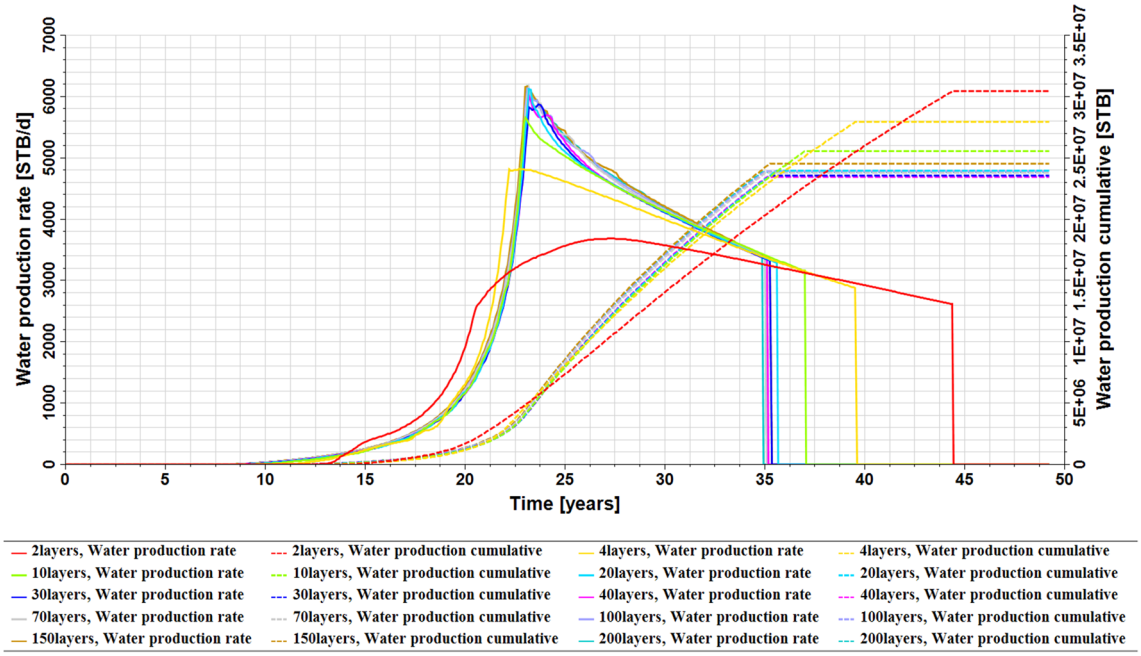

Fig. 11 Water production rate and cumulative water production for models with different layers

feet (one-half of total reservoir thickness) beginning at the top of the reservoir. The reservoir was produced on a maximum-gas-production-rate constraint of 50 MMscf/day and a minimum THP constraint of 738 psia. The well was shut in when the minimum gas production rate was less than 2.0 MMscf/day or the maximum water–gas ratio (WGR) was more than 1000 STB/MMscf. The base radial simulation model is displayed in Fig. 17. The studied factors were gas production rate, completion length, aquifer size, reservoir horizontal permeability, and permeability anisotropy. Each factor was assigned a plausible range, as summarized in Table 5.

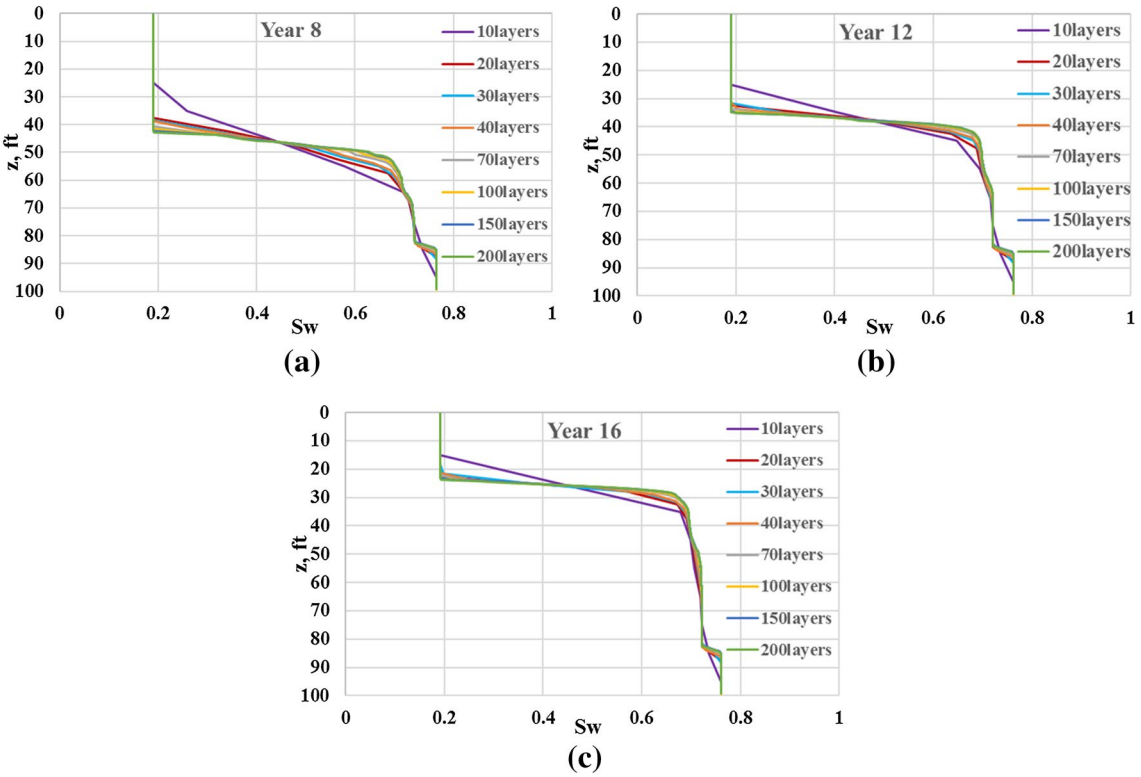

Fig. 12 Water saturation profile at near wellbore along vertical depth for models with different layers at three different production times

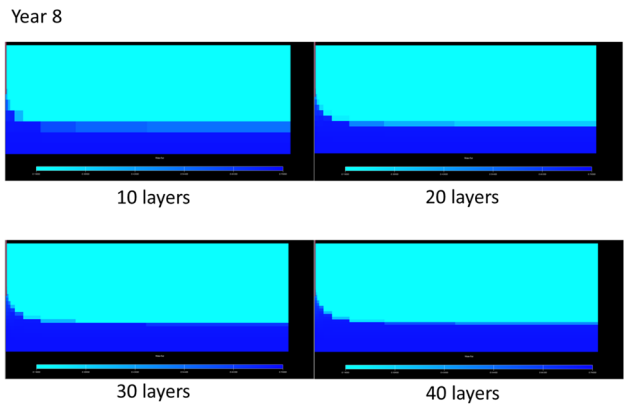

Fig. 13 Water saturation profile along a reservoir radius for 4 models with different layers after 8-year production

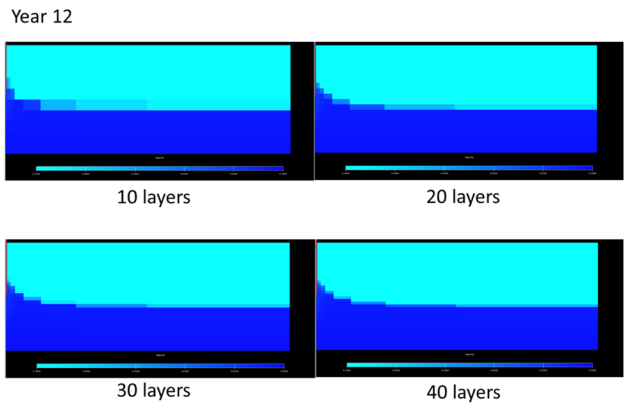

Fig. 14 Water saturation profile along a reservoir radius for 4 models with different layers after 12-year production

Gas production rate

The well was produced at gas rate from 10 to 150 MMscf/day. The simulated performance is shown in Figs. 18, 19, and 20. In general, with a smaller gas production rate, the gas-production-plateau period increases, which prolongs field production life. With a specific field production strategy, a minimum gas production rate is required to recover all the reserves before the end of field life. In this study, with the field life of 20 years, the minimum gas production rate is approximately 16 MMscf/day. Figure 21 shows the gas and oil recoveries for different gas production rates. As the gas production rate increases, the gas recovery is almost the same, while the oil recovery tends to decrease. As displayed in Fig. 22, the total water production increases when the gas rate increases up to 60 MMscf/day. After that, the total water production does not change with increasing gas production rate. The change in gas production rate not

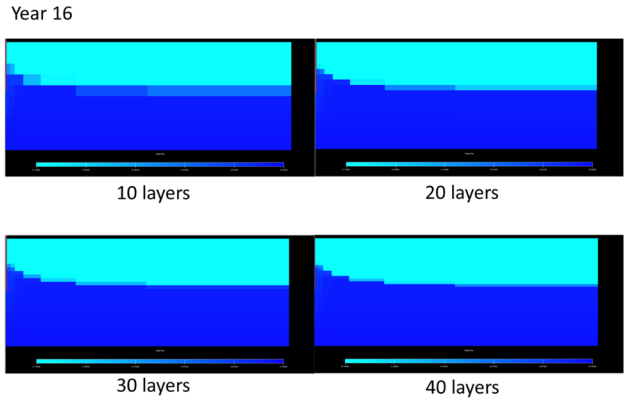

Fig. 15 Water saturation profile along a reservoir radius for 4 models with different layers after 16-year production

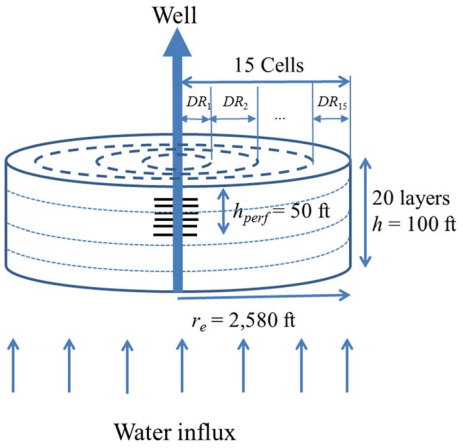

Fig. 17 General view of base fine-grid radial simulation model for sensitivity study

only influences the field production life but also the water breakthrough time. Both field production life and water breakthrough time rapidly decline when gas production rate increases from 10 to 60 MMscf/day, as indicated in Fig. 23. When the gas production rate is greater than 60 MMscf/day, both field production life and water breakthrough time do not change much with increasing gas rate.

Table 5 Studied range of production and reservoir factors

Factor	Symbol	Unit	Range
Gas production rate	q_g	MMscf/day	10–150
Completion length	$h_{pD} = h_{perf}/h$		0.05–1
Aquifer size	$M = V_{aq}/PV_g$		0.5–30
Horizontal permeability	k_H	mD	100–800
Permeability anisotropy	k_V/k_H		0.1–1

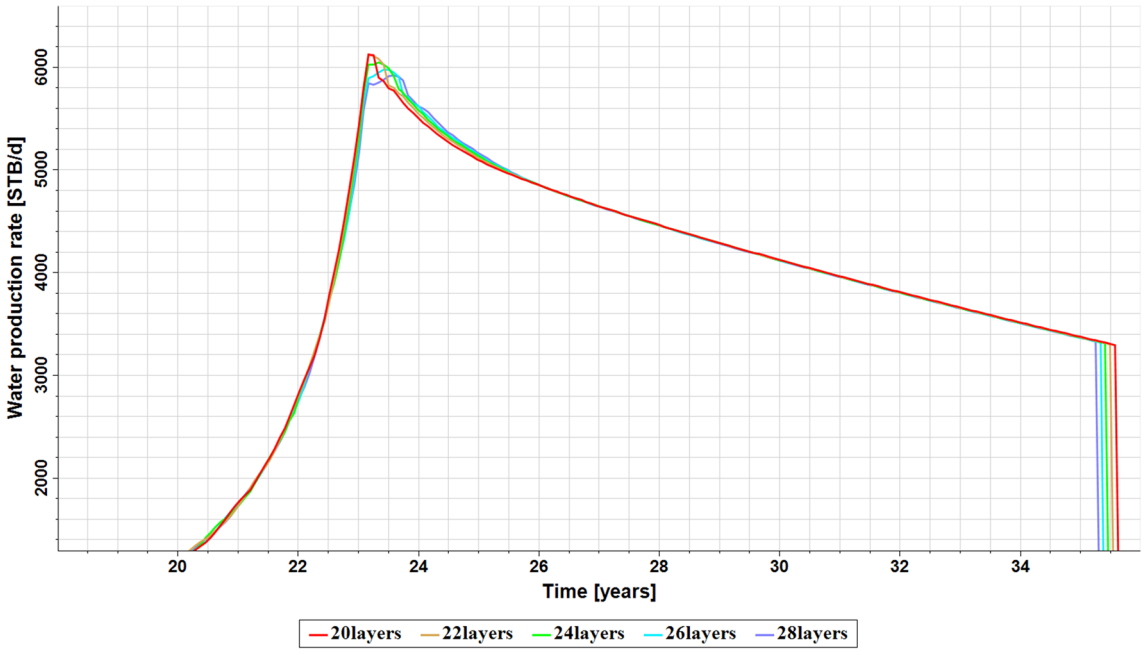

Fig. 16 Water production rate for models with 20–28 layers

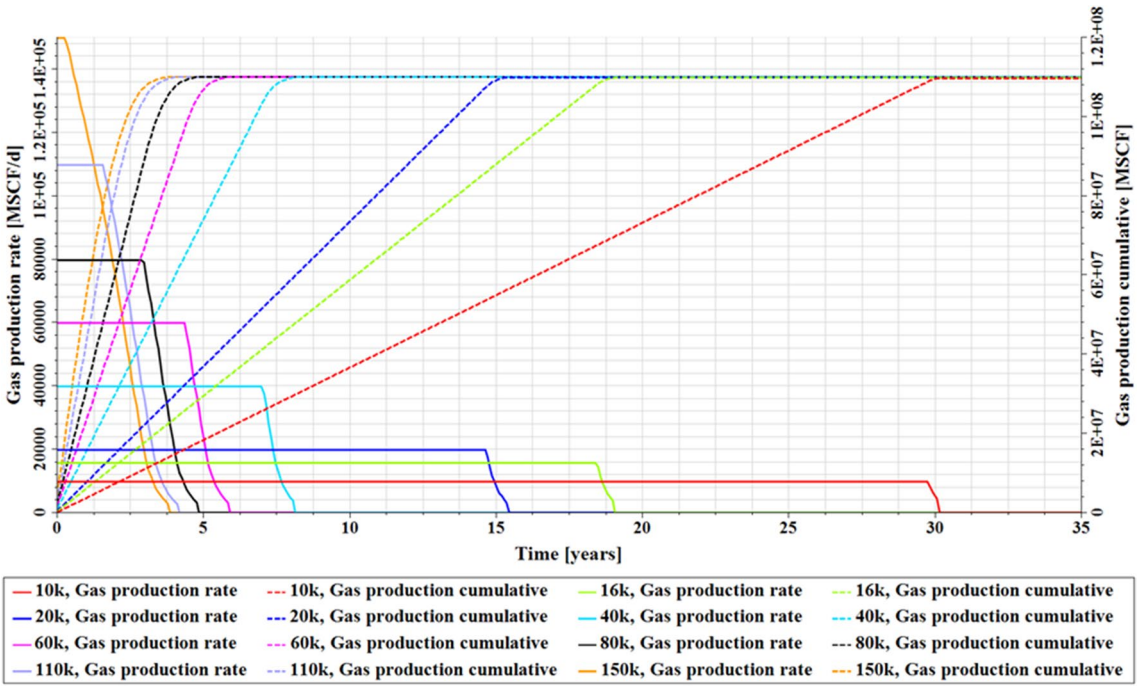

Fig. 18 Gas productions vs. time for different gas production rates

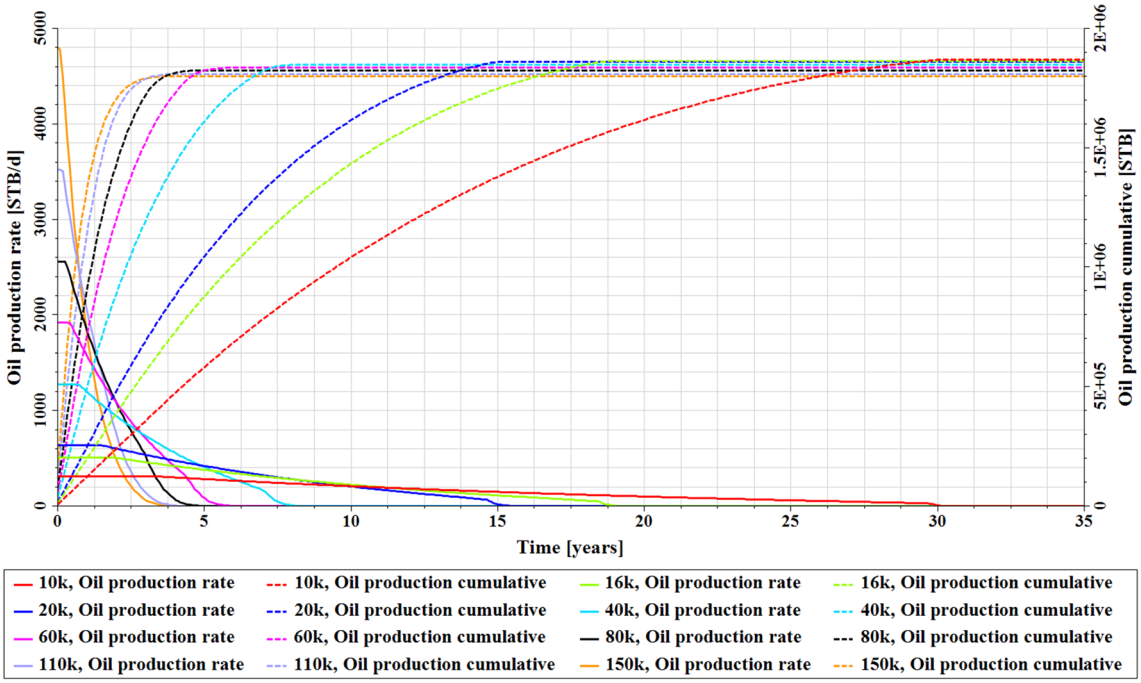

Fig. 19 Oil productions vs. time for different gas production rates

Completion length

In this study, the completion length ($h_{pD} = h_{perf}/h$) covered a continuous interval from the top of the reservoir, with a range from 0.05 to 1.0. Figures 24, 25, and 26 show the simulated production results for different completion lengths. With $h_{pD} \leq 0.4$, an increase in completion length results in an increase in both gas and oil recoveries and

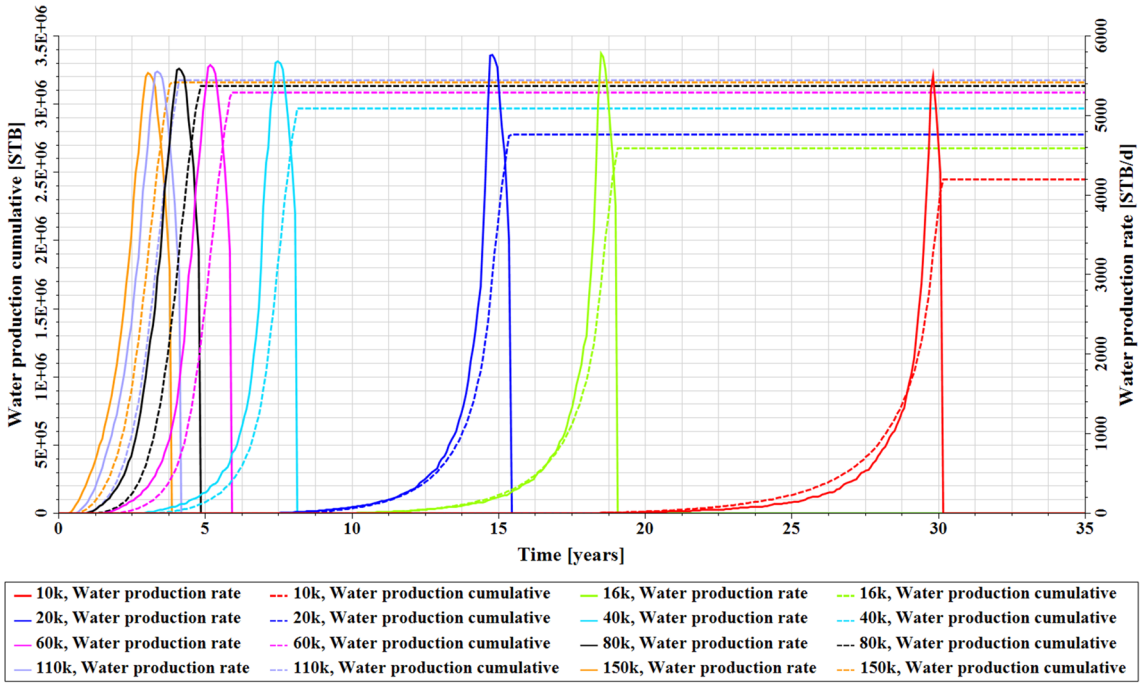

Fig. 20 Water productions vs. time for different gas production rates

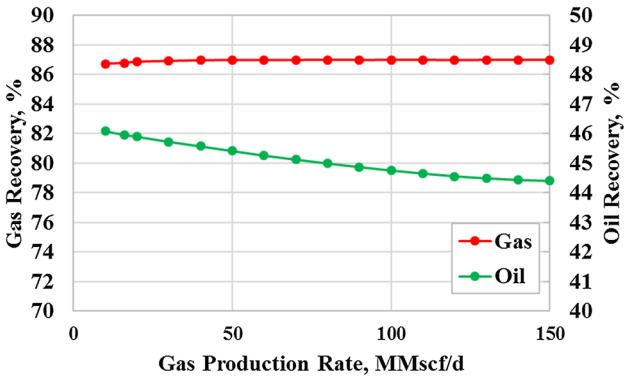

Fig. 21 Gas and oil recoveries for different gas production rates

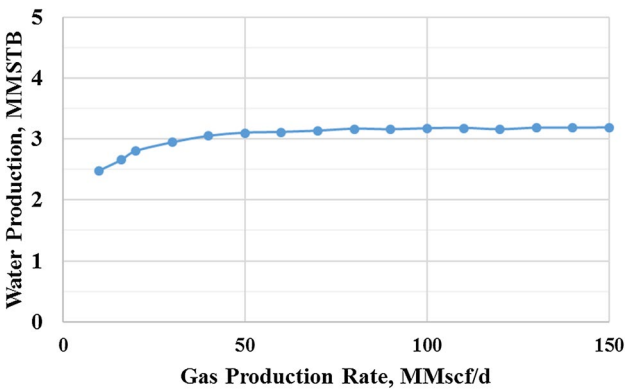

Fig. 22 Total water production for different gas production rates

total water production. When $h_{pD} > 0.4$, the oil recovery slightly decreases with increasing h_{pD}, while gas recovery and total water production are almost the same for any completion length. Moreover, the higher the completion length is, the shorter the field production life becomes and the faster the water breakthrough occurs. To maximize gas and oil recoveries for Sand20, the completion length is recommended to be around 0.4.

Aquifer size

Aquifer size determines the amount of reservoir energy that can be provided by water influx. In this study, the aquifer size, M, varied from 0.5 to 30. Figures 27, 28, and 29 show the simulated production results for different aquifer sizes. As indicated in Fig. 27, oil recovery monotonically increases with increasing aquifer size. However, gas recovery reaches a maximum at $M \approx 10$ and then decreases with increasing aquifer size. Field production life is also maximum at $M \approx 10$, as displayed in Fig. 29. Figures 28 and 29 show that when $M \leq 4$, there is no water production during field life. When $4 \leq M \leq 15$, water breakthrough occurs earlier and total water production rapidly increases with higher aquifer size. When $M \geq 15$, there is no difference in water breakthrough time. Total water production slightly reduces in the beginning then remains unchanged.

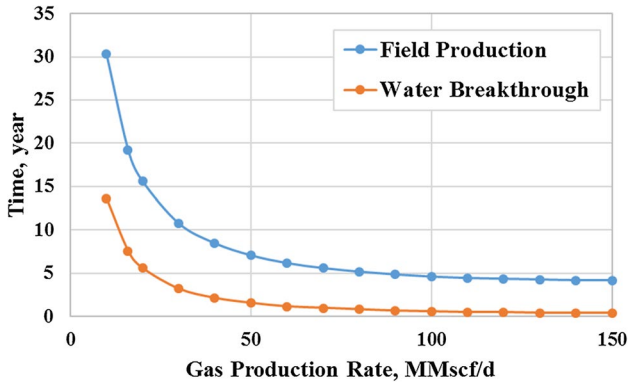

Fig. 23 Field production life and water breakthrough time for different gas production rates

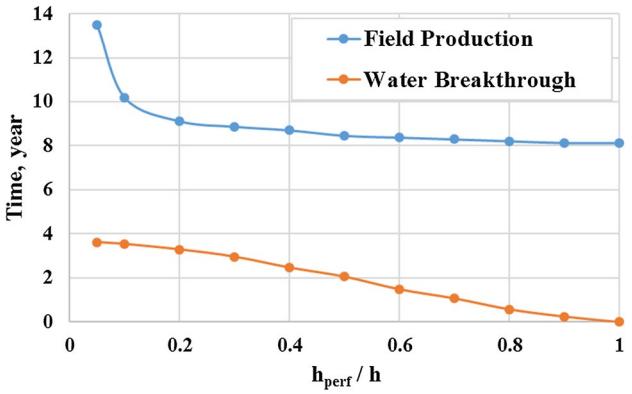

Fig. 26 Field production life and water breakthrough time for different completion lengths

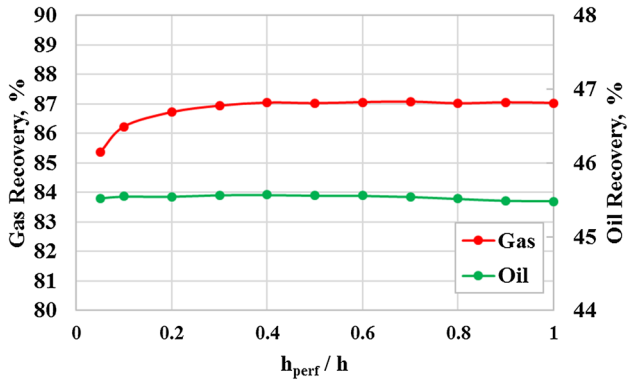

Fig. 24 Gas and oil recoveries for different completion lengths

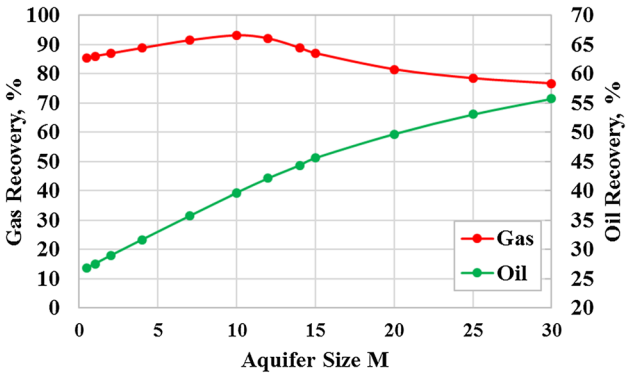

Fig. 27 Gas and oil recoveries for different aquifer sizes

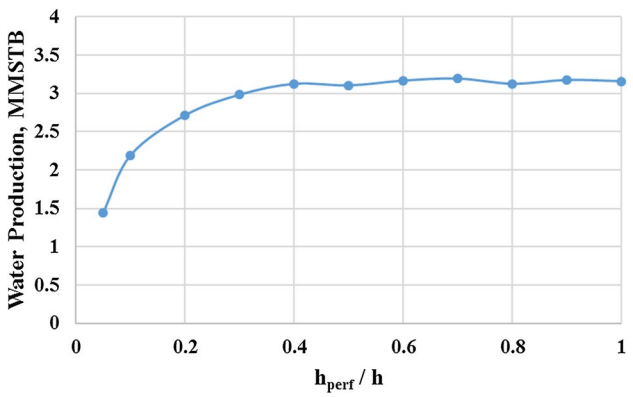

Fig. 25 Total water production for different completion lengths

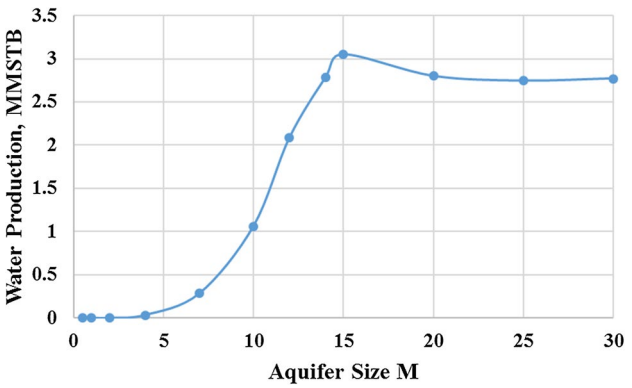

Fig. 28 Total water production for different aquifer sizes

Reservoir horizontal permeability

The reservoir horizontal permeability was studied in the range from 100 to 800 mD. Figure 30 displays the ultimate gas and oil recoveries for different horizontal permeabilities and production rates. There is a negligible change in the gas and oil recoveries between horizontal permeability of 400 and 800 mD. When the horizontal permeability reduces from 400 to 100 mD, both gas and oil recoveries decrease. The reductions in gas and oil recoveries are approximately 4 and 1%, respectively. Figures 31 and 32 show that for the same gas rate, as the reservoir horizontal permeability decreases from 800 to 100 mD, the total water production increases,

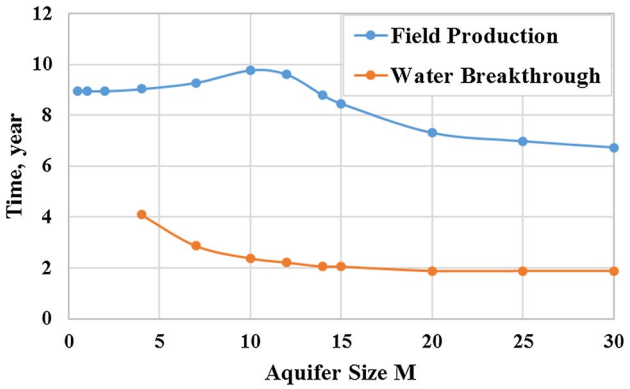

Fig. 29 Field production life and water breakthrough time for different aquifer sizes

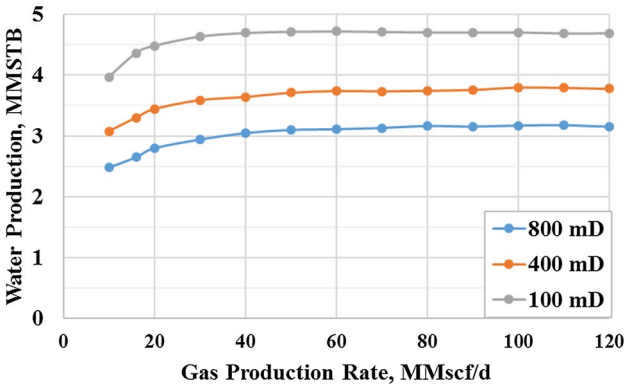

Fig. 31 Total water production for different horizontal permeabilities at various aquifer sizes

the water breakthrough occurs earlier, and the field production life becomes longer. Moreover, as indicated in Fig. 30, for each reservoir horizontal permeability, the gas recoveries are practically independent of gas production rate, while the oil recoveries slightly decrease with increasing gas rate.

Permeability anisotropy

The permeability anisotropy was also considered in this study. The vertical-to-horizontal permeability ratio was varied in the range from 0.1 to 1.0. Figures 33, 34, and 35 show the simulated results for different vertical-to-horizontal permeability ratio. In general, the gas and oil recoveries are almost the same. An increase in vertical-to-horizontal permeability ratio results in a small increase in the total water production of approximately 1%. As indicated in Fig. 35, permeability anisotropy has negligible effects on the field production life. However, increasing permeability anisotropy ratio leads to a slightly earlier water breakthrough.

Water–gas ratio

In the base case, the well was perforated with an interval of 50 ft, which was a half of the total thickness. With the thickness of each layer of 5 ft, the total perforated cells was 10. Figure 36 displays the water saturation of top 10% (the topmost perforated cell) at near wellbore and water–gas ratio (WGR) with time at three different production rates. As shown in Fig. 36, when the topmost perforated cell starts to be flooded with water (a sudden increase in water saturation), the WGR increases rapidly from 0.1 to 1.0 STB/ Mscf.

Similar results were observed when the whole reservoir was perforated, as shown in Fig. 37. From these results, it could be seen that water–gas ratio does not increase rapidly until approximately 90% of perforation interval is flooded with water.

Conclusions

In this study, a benchmarked radial simulation model was constructed for a gas-condensate reservoir with bottom water influx by calibrating with analytical solution and

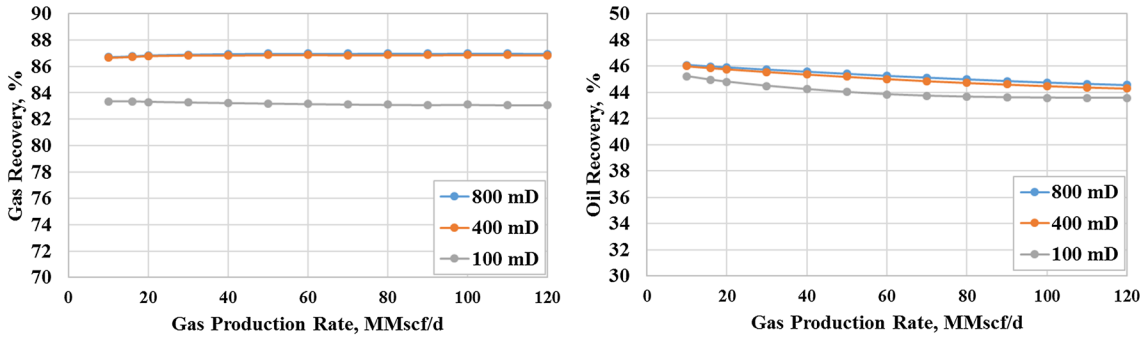

Fig. 30 Gas and oil recoveries for different horizontal permeabilities at various production rates

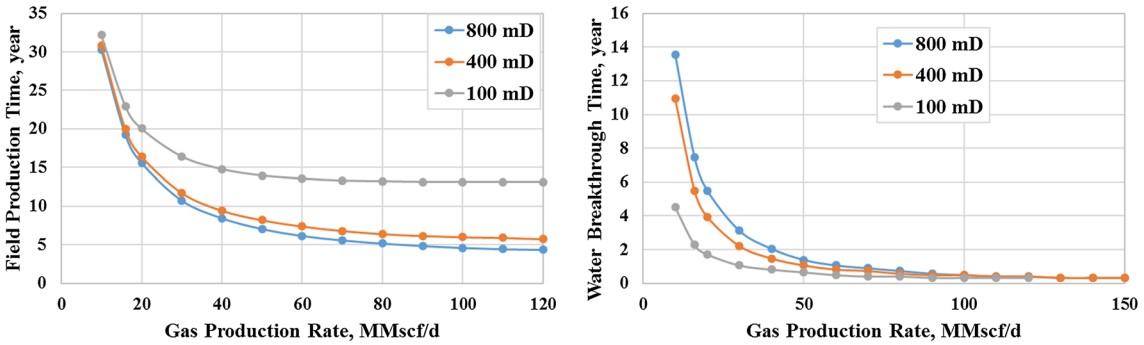

Fig. 32 Field production life and water breakthrough time for different reservoir horizontal permeabilities at various production rates

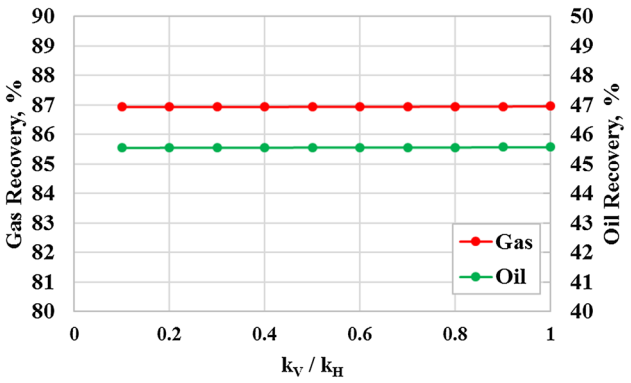

Fig. 33 Gas and oil recoveries for different vertical-to-horizontal permeability ratios

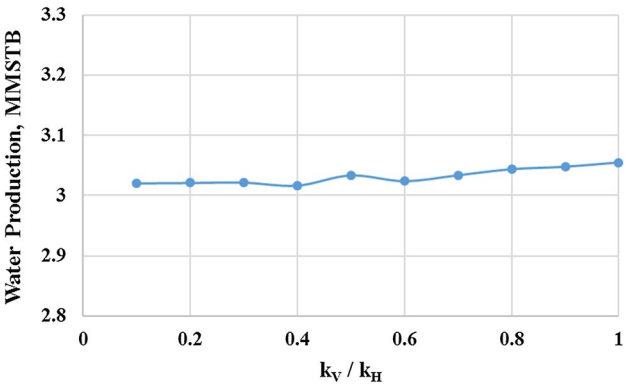

Fig. 34 Total water production for different vertical-to-horizontal permeability ratios

performing convergence tests. In addition, the workflow to analyze the effects of bottom water influx on similar gas-condensate reservoirs was established.

The effects of production and reservoir factors on recovery and production behaviors of a gas-condensate sandstone reservoir Sand20 offshore Vietnam were also investigated. The following conclusions were made from the study:

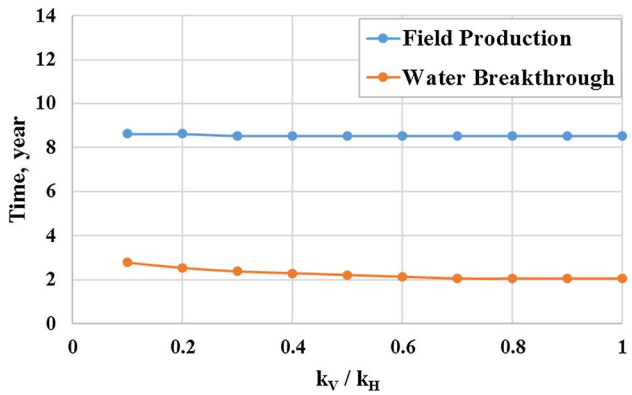

Fig. 35 Field production life and water breakthrough time for different vertical-to-horizontal permeability ratios

1. Gas production rate has negligible influence on gas recovery. To maximize the ultimate oil recovery, minimize total water production, delay water breakthrough time, and prolong field production life, the well should be produced at low gas rates. However, with a specific field life, a minimum gas production rate is required to recover all the reserves before abandonment. For Sand20, the minimum gas production rate was found to be approximately 16 MMscf/day for the field life of 20 years.
2. The gas and oil recoveries and total water production increase with increasing completion length when $h_{perf}/h \leq 0.4$. When $h_{perf}/h > 0.4$, an increase in h_{perf}/h ratio results in small decrease in oil recovery and no change in both gas recovery and total water production. The higher the completion length is, the shorter field production life becomes and the faster the water breakthrough occurs. Therefore, for Sand20 gas-condensate reservoir, the completion length should be roughly 0.4 to maximize the gas and oil recoveries.
3. The oil recovery increases with the size of aquifer, while the gas recovery and field production life are maximum when the aquifer is approximately ten times larger than

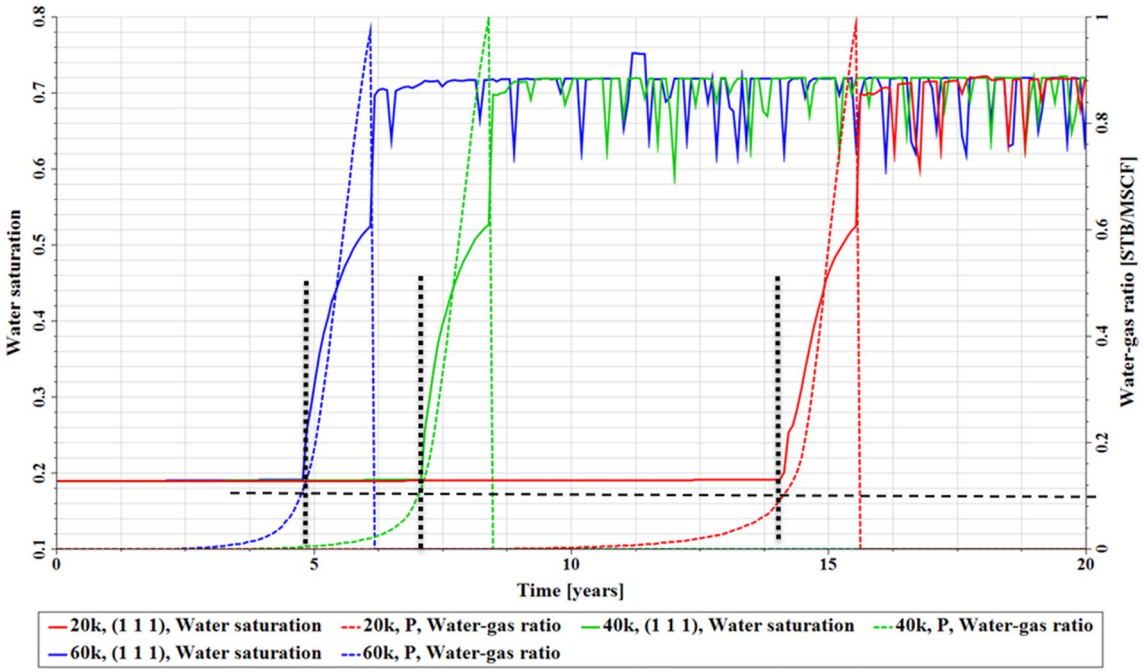

Fig. 36 Water saturation of the top 10% of perforation interval and WGR vs. time at three different production rates, $h_{pD} = 0.5$

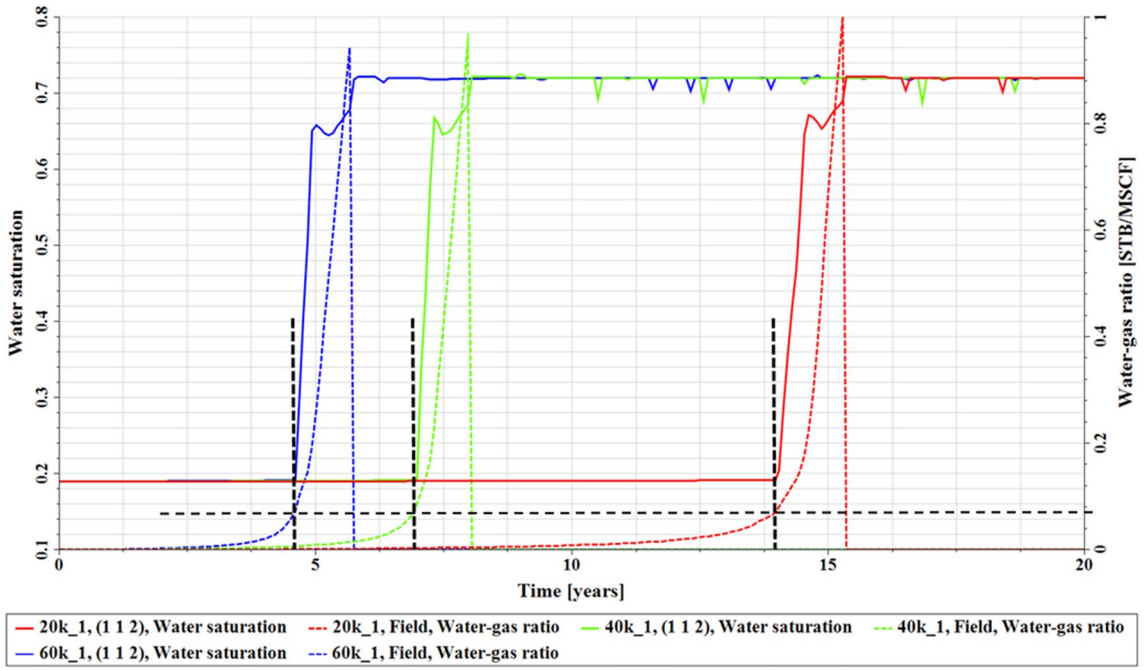

Fig. 37 Water saturation of the top 10% of perforation interval and WGR vs. time at three different production rates, $h_{pD} = 1.0$

pore volume of reservoir fluid. For $M \leq 15$, increasing aquifer size leads to higher water production and earlier water breakthrough. However, when $M > 15$, aquifer size has little impacts on both water production and water breakthrough time.

4. The recoveries are almost the same for reservoirs with horizontal permeability of 400 and 800 mD. When permeability reduces to 100 mD, the reduction in recoveries are around 1–4%. Moreover, as the reservoir horizontal permeability decreases from 800 to 100 mD, the total

water production and the field production life increase, while the water breakthrough time decreases. For a gas-condensate reservoir with permeability greater than 100 mD, the gas production rate has negligible influences on the gas recovery, while the oil recovery slightly decreases with increasing gas production rate.

5. The permeability anisotropy has negligible effects on both gas and oil recoveries as well as field production life. There is only a small increase of approximately 1% in total water production when permeability ratio increases from 0.1 to 1. The water breakthrough is likely to occur earlier with a large vertical-to-horizontal permeability ratio.
6. From the simulated results, WGR does not increase rapidly until approximately 90% of perforation interval is flooded with water.

The results in this study are specific for Sand20 gas-condensate reservoir, and may be not representative for other reservoirs. However, the proposed workflow can be used to study other gas-condensate reservoirs under bottom water influx.

Acknowledgements The authors would like to thank Bien Dong POC (BDPOC), PetroVietnam (PVN), and Gazprom EP International B.V. (GPEPI) for permission to publish this paper.

References

Agarwal RG, Al-Hussainy R, Ramey HJ Jr (1965) The importance of water influx in gas reservoirs. J Pet Technol 17(11):1336–1342. https://doi.org/10.2118/1244-PA (SPE-1244-PA)

Ali F (2014) Importance of water influx and water flooding in gas-condensate reservoir. MS thesis, Norwegian University of Science and Technology, Trondheim

Armenta M (2003) Mechanisms and control of water inflow to wells in gas reservoirs with bottom-water drive. Ph.D dissertation, Lousiana State University, Baton Rouge

Banum RS, Brinkman FP, Richardson TW et al (1995) Gas condensate reservoir behaviour: productivity and recovery reduction due to condensation. In: Presented at the SPE annual technical conference and exhibition, Dallas, 22–25 October. https://doi.org/10.2118/30767-MS (**SPE-30767-MS**)

El-Banbi AH, McCain WD Jr, Semmelbeck ME (2000) Investigation of well productivity in gas-condensate reservoirs. In: Presented at the SPE/CERI gas technology symposium, Calgary, 3–5 April. https://doi.org/10.2118/59773-MS (**SPE-59773-MS**)

Fevang Ø, Whitson CH (1996) Modeling gas condensate well deliverability. SPE Res Eng 11(4):221–230. https://doi.org/10.2118/30714-PA (SPE-30714-PA)

Hinchman SB, Barree RD (1985) Productivity loss in gas condensate reservoirs. In: Presented at the SPE annual technical conference and exhibition, Las Vegas, 22–25 September. https://doi.org/10.2118/14203-MS (**SPE-14203-MS**)

Hower TL, Lewis DR, Owens RW (1992)Recovery optimization in a multi-reservoir offshore gas field with water influx. In: Presented at the SPE Annual Technical Conference and Exhibition, Washington, 4–7 October. https://doi.org/10.2118/24865-MS (**SPE-24865-MS**)

Izuma NC, Nwosu CN (2014) Influence of aquifer support on gas condensate reservoir performance. In: Presented at the Nigeria annual international conference and exhibition, Lagos, 5–7 August. https://doi.org/10.2118/172372-MS (**SPE-172372-MS**)

Ogolo NA, Isebor JO, Onyekonwu M (2014) Feasibility study of improved gas recovery by water influx control in water drive gas reservoirs. In: Presented at the Nigeria annual international conference and exhibition, Lagos, 5–7 August. https://doi.org/10.2118/172364-MS (**SPE-172364-MS**)

Singh K, Whitson CH (2010) Gas-condensate pseudopressure in layered reservoirs. SPE Res Eval Eng 13(2):203–213. https://doi.org/10.2118/117930-PA (SPE-117930-PA)

Tran TV, Ngo AT, Hoang HM, Tran NH 2015. Production performance of gas condensate reservoirs—compositional numerical model—a case study of Hai Thach—Moc Tinh Fields. In: Presented at the Abu Dhabi international petroleum exhibition and conference, Abu Dhabi, 9–12 November. https://doi.org/10.2118/177445-MS (**SPE-177445-MS**)